An RBF–Galerkin approach to the time-dependent Schrödinger equation

Katharina Kormann* Elisabeth Larsson*

Abstract

In this article, we consider the discretization of the time-dependent Schrödinger equation using radial basis functions (RBF). We formulate the discretized problem over an unbounded domain without imposing explicit boundary conditions. Since we can show that time-stability of the discretization is not guaranteed for an RBF-collocation method, we propose to employ a Galerkin ansatz instead. For Gaussians, it is shown that exponential convergence is obtained up to a point where a systematic error from the domain where no basis functions are centered takes over. The choice of the shape parameter and of the resolved region is studied numerically. Compared to the Fourier method with periodic boundary conditions, the basis functions can be centered in a smaller domain which gives increased accuracy with the same number of points.

Key words. radial basis function, partial differential equation, Galerkin method, time-dependent Schrödinger equation

1 Introduction

The simulation of quantum dynamical processes by the time-dependent Schrödinger equation (TDSE) reveals the dynamics of chemical bonds and reactions. Two main challenges when numerically solving the TDSE are the curse of dimensionality and the unboundedness of the domain. The number of degrees of freedom in a quantum mechanical system is about three times the number of particles. Hence, the number of equations describing the TDSE discretized with a grid-based method will increase exponentially with the number of particles. Adaptivity has been used in both finite element [8, 31] and finite difference methods [40, 24] in order to reduce the number of grid points. Another direction is to reduce the number of basis functions needed to describe the system by exploiting classical properties of the system. In its simplest form such a semiclassical method approximates the initial wave packet with a number of complex Gaussians, so-called coherent states, whose positions and momenta are then propagated along classical trajectories [25]. More sophisticated variants have been developed over the years (see e.g. [2, 49, 55, 11]). While semiclassical methods enable computations for comparably large systems, many times they render it difficult to detect complex quantum-mechanical phenomena. To some extent, coherent states

*Division of Scientific Computing, Department of Information Technology, Uppsala University, Box 337, 751 05 Uppsala, Sweden (katharina.kormann@it.uu.se, elisabeth.larsson@it.uu.se).

resemble Gaussian radial basis functions (which however do not include a phase), which are studied within the literature on radial basis functions (RBF) approximations of partial differential equations (PDE) (see [4, 54, 12] and references therein). In RBF approximation the width of the Gaussians is chosen to minimize the approximation error [45, 5, 35] as opposed to in the semiclassical case where the width is coupled to properties of the physical problem. RBFs yield highly accurate approximations for smooth solutions (cf. e.g. [54, Ch. 11] and [44]), similarly to pseudospectral methods (see [14, 33, 51, 23, 10] for spectral methods applied to the TDSE). Contrary to the latter method, however, RBFs are mesh tolerant [36, 9]. This offers generality in node placement when going to higher dimensions where pseudospectral methods are limited to tensor product grids. Admittedly, this comes with the price that fast transform methods are generally not available. In addition to this flexibility, the resemblance to semiclassical methods might be a starting point for hybrid methods designed to simulate complicated quantum phenomena in larger molecules.

RBF discretizations of PDEs are mostly implemented as collocation methods [30], the reason being difficulties in accurately computing the integrals in Galerkin methods. For time-dependent PDEs, it is however common that stability problems arise. In [42], the existence of spurious eigenvalues due to the introduction of boundary conditions was reported. We demonstrate that such instabilities arise also in our setting due to a variable coefficient term in the TDSE. Therefore, we propose a Galerkin formulation for the TDSE. The integrals are evaluated analytically which becomes possible since we do not impose explicit boundaries. For this formulation, we show stability and convergence. Also, we numerically analyze how the parameters in our method should be chosen and how sensitive the approximation is to variations in the parameters. In a comparison with the Fourier pseudospectral method and RBF-collocation, we demonstrate the high accuracy of our method. We concentrate on the Schrödinger equation in this article but the approach potentially applies for instance to problems described by the Fokker–Planck equation in finance, systems biology, and plasma physics.

RBF interpolation using a Galerkin ansatz in an unbounded domain was also used in [27]. Sarra [47] demonstrated that collocation with Gaussian radial basis functions for infinite-domain problems can be efficiently implemented when restricting the node distribution to a uniform mesh for the example of the Gross–Pitaevskii equation. Radial basis functions have been used for the solution of the Schrödinger eigenvalue problem (see, e.g., [6, 28, 37]). In [7], a two dimensional time-dependent Schrödinger equation with Dirichlet boundary conditions was discretized using radial basis function collocation, but no stability analysis was provided. Radial basis functions were also applied for the solution of the equations from quantum fluid dynamics in [29].

The outline of the article is as follows. In the next section, we introduce RBF approximation of the TDSE both for collocation and Galerkin methods. We also explain the boundary treatment and temporal propagation with an exponential integrator. Sec. 3 considers stability and in Sec. 4 we show exponential convergence provided that the solution is small enough outside the domain where the basis functions are centered. We explain in Sec. 5 how to interpolate between different basis sets which is necessary when dynamic mesh refinement is used. The choice of the computational domain and the shape parameter are studied in Sec. 6, and a comparison of our method to RBF-

collocation and the popular Fourier method is provided in Sec. 7. Sec. 8 concludes the article.

2 Radial Basis Function Approximation of the TDSE

The time-dependent Schrödinger equation (TDSE) is given as

$$\mathrm{i}\hbar\frac{\partial}{\partial t}\Psi(x,t) = \widehat{H}\Psi(x,t), \quad \Psi(x,0) = \Psi_0, \tag{1}$$

where $\hat{H} = \hat{T}(\frac{\partial^2}{\partial x_1^2},\dots,\frac{\partial^2}{\partial x_d^2}) + \hat{V}(x)$ is the molecular Hamiltonian for d degrees of freedom, consisting of the kinetic ($\hat{T}$) and the potential ($\hat{V}$) energy operator of the system. Equation (1) is solved for the wave function $\Psi \in L_2(H^1(\mathbb{R}^d)\times J)$, $\frac{\partial}{\partial t}\Psi \in L^2(H^{-1}(\mathbb{R}^d)\times J)$, where $J = (0,t_{\text{final}}]$ and $0 < t_{\text{final}} < \infty$, with some given $\Psi_0 \in H^1(\mathbb{R}^d)$. Here, L_2 denotes the space of square integrable functions and H^1 the space of functions that are square integrable and have square integrable first derivatives. The dual space of $H^1(\mathbb{R}^d)$ is denoted by $H^{-1}(\mathbb{R}^d)$.

The shape of the potentials $\hat{V}$ can be highly diverse. There are a number of functions that are often used in simulations since they model typical energy configurations. On the other hand, it is also common that the value of the potential is known only at a number of discrete points. In the latter case, we consider it suitable to use RBF interpolation to approximate the potential. Then, the Galerkin matrices can easily be evaluated analytically.

In this paper, we will consider two different potentials. Firstly, we consider the harmonic oscillator where we have a quadratic potential,

$$V(x) = \sum_{k=1}^{d}\frac{1}{2}m_k\omega_k^2x_k^2.$$

This model is rather simple but nevertheless of importance in quantum dynamics since it models the shape of more complicated potentials close to a stable equilibrium [22, Ch. 2.3]. Analytical solutions can be constructed in this example for verification of the numerical results. A family of solutions is given by

$$\psi(x,t) = C\exp\left(-\sum_{k=1}^{d}\beta_k(x_k-x_{k,t})^2 + \frac{\mathrm{i}}{\hbar}\sum_{k=1}^{d}p_{k,t}(x_k-x_{k,t}) + \frac{\mathrm{i}}{\hbar}\sum_{k=1}^{d}\gamma_{k,t}\right),$$

where $x_{k,t} = x_{k,0}\cos(\omega_k t) + p_{k,0}/(m_k\omega_k)\sin(\omega_k t)$, $\beta_k = \frac{m_k\omega_k}{2\hbar}$, $p_{k,t} = p_{k,0}\cos(\omega_k t) - x_{k,0}m_k\omega_k\sin(\omega_k t)$ and $\gamma_{k,t} = \frac{1}{2}\left(p_{k,t}x_{k,t} - p_{k,0}x_{k,0} - \hbar\omega_k t\right)$. If not stated otherwise, we consider the problem in one dimension and start at the origin with $p_{1,0} = 2$, $m = 1$, $\omega = 1$. Secondly, we consider the modified Hénon–Heiles potential in two dimensions,

$$V(x_1,x_2) = \frac{x_1^2}{2} + \frac{x_2^2}{2} + \sigma\left(x_1^2x_2 - \frac{x_2^3}{3}\right) + \frac{\sigma^2}{16}\left(x_1^2+x_2^2\right)^2, \tag{2}$$

with a positive parameter σ. The Hénon–Heiles potential appeared originally in astrophysics and was introduced in this modified form to quantum dynamics as a model of coupled oscillators [34].

A radial basis function approximation [4, 54, 12] is based on a radial function $\varphi(r)$, $r \in \mathbb{R}_+$, a set of center points $X = \{c_1, \ldots, c_N\} \subset \mathbb{R}^d$, and a shape parameter ε. The approximant is then defined as

$$s(x) = \sum_{j=1}^{N} \lambda_j \varphi_\varepsilon(\|x - c_j\|), \tag{3}$$

where $\varphi_\varepsilon(r) = \varphi(\varepsilon r)$ and $\lambda_j \in \mathbb{C}$ are coefficients. Also, the shape parameter can be varied. In particular, we define the interpolant I_f of some function f to be the function of the form (3) where the coefficients are determined such that $I_f(c_j) = f(c_j)$ for all $c_j \in X$.

Moreover, let us denote by q the *separation radius*

$$q := \frac{1}{2} \min_{c,d \in X, c \neq d} \|c - d\|,$$

i.e., half the smallest distance between center points. For a compact, connected region $\Omega \in \mathbb{R}^d$, we define the *fill distance* h for Ω relative to X to be the maximum distance of a point from Ω to the set X,

$$h := \sup_{x \in \Omega} \min_{c \in X} \|x - c\|. \tag{4}$$

2.1 Collocation approach

In order to discretize the TDSE based on radial basis function collocation, one may take the ansatz

$$\psi(x,t) = \sum_{k=1}^{N} \lambda_k(t) \varphi_\varepsilon(\|x - c_k\|), \tag{5}$$

where $c_k \in \mathbb{R}^d$ are suitably chosen center points. Inserting this ansatz into the TDSE (1) and evaluating the TDSE at given evaluation points q_j gives the collocation discretization

$$A \frac{\mathrm{d}}{\mathrm{d}t} \lambda = -\frac{\mathrm{i}}{\hbar} H \lambda,$$

where

$$A_{j,k} = \varphi_\varepsilon(\|q_j - c_k\|), \qquad H_{j,k} = -\sum_{i=1}^{d} \frac{\hbar^2}{2m_i} \frac{\partial^2}{\partial x_i^2} \varphi_\varepsilon(\|q_j - c_k\|) + V(q_j) \varphi_\varepsilon(\|q_j - c_k\|).$$

Let us also introduce the matrices $\Lambda = \mathrm{diag}(V(q_1), \ldots V(q_N))$ and S with

$$S_{j,k} = -\sum_{i=1}^{d} \frac{\hbar^2}{2m_i} \frac{\partial^2}{\partial x_i^2} \varphi_\varepsilon(\|q_j - c_k\|).$$

Then, it holds that $H = S + \Lambda A$. Note that if the sets of center and evaluation points coincide, the matrices A and S are symmetric.

2.2 Galerkin approach

An alternative approach is to base the approximation on the weak form of the TDSE,

$$\mathrm{i}\hbar\left(\Phi, \frac{\partial}{\partial t}\Psi\right) = \sum_{i=1}^{d} \frac{\hbar^2}{2m_i}\left(\frac{\partial}{\partial x_i}\Phi, \frac{\partial}{\partial x_i}\Psi\right) + (\Phi, V\Psi) \quad \text{for all } \Phi \in H^1(\mathbb{R}^d). \tag{6}$$

By $(\cdot,\cdot)$, we denote the $L_2(\mathbb{R}^d)$ inner product. Approximating (6) in the finite dimensional subspace spanned by the basis functions in (5) and letting Ψ be approximated by ψ yields the Galerkin discretization of the TDSE

$$M\frac{\mathrm{d}}{\mathrm{d}t}\lambda = -\frac{\mathrm{i}}{\hbar}G\lambda, \tag{7}$$

where

$$\begin{aligned} M_{j,k} &= \int_{\mathbb{R}^d} \varphi_\varepsilon(\|x-c_j\|)\varphi_\varepsilon(\|x-c_k\|)\,\mathrm{d}x, \\ G_{j,k} &= \int_{\mathbb{R}^d} \sum_{i=1}^{d} \frac{\hbar^2}{2m_i}\frac{\partial}{\partial x_i}\varphi_\varepsilon(\|x-c_j\|)\frac{\partial}{\partial x_i}\varphi_\varepsilon(\|x-c_k\|) \\ &\quad + \varphi_\varepsilon(\|x-c_j\|)V(x)\varphi_\varepsilon(\|x-c_k\|)\,\mathrm{d}x. \end{aligned} \tag{8}$$

In order to evaluate the *stiffness matrix G* and the *mass matrix M* for the Galerkin approximation, we need to compute integrals over $\mathbb{R}^d$. This requires that the chosen radial basis functions and their first derivatives are square integrable. Moreover, the product induced by the potential has to be finite. Common RBF functions, like multiquadrics, inverse multiquadrics, inverse quadrics, thin plate splines, and piecewise polynomials, are not square integrable on the whole $\mathbb{R}^d$. Gaussians as well as compactly supported basis functions like Wendland functions [52], on the other hand, are square integrable and have finite moments.

The Gaussian basis is a radial basis function that is suited for a Galerkin approximation in infinite domains. The ansatz function is given as

$$\varphi_\varepsilon(r) = \left(\frac{2\varepsilon^2}{\pi}\right)^{\frac{d}{4}} \exp\left(-(\varepsilon r)^2\right). \tag{9}$$

Gaussians are in $H^1(\mathbb{R}^d)$ and all moments are finite. Moreover, one can find analytical expressions for the moments. Hence, both the mass and stiffness matrices can be evaluated analytically as long as the potential is a polynomial or itself interpolated by Gaussian RBFs. In the appendix, we give the analytical expressions for some moments and the negative Laplacian. For an example of how Wendland functions can be used in a Galerkin approach, see [53].

2.3 Boundary conditions

In its general form the TDSE is posed in the whole space and the requirement $\Psi \in H^1(\mathbb{R}^d)$ implicates decay towards infinity. The integrability assumption replaces explicit boundary conditions. For numerical simulations, it is common to truncate the computational domain such that the probability for the particle to leave the computational domain is below a certain (low) tolerance over the whole simulation time. In

this case periodic or homogeneous Dirichlet boundary conditions are common. The former condition suffers from unphysical leakage from one side of the domain to the other and the latter from (small) reflections from the boundary. Which formulation is chosen depends on the ease of implementation for the chosen discretization method. For instance, periodic boundary conditions are typically selected in combination with Fourier-pseudospectral methods [14, 33]. While this works quite well for models of bound states, the computational domain might get too large when dissociative problems are modeled. In this case, various kinds of absorbing boundary conditions are commonly used [1]. Alternatively, spectral methods can be formulated in the whole $\mathbb{R}^d$ with Hermite basis functions that decay sufficiently fast towards infinity [10]. This allows for a formulation of the discrete problem without explicit boundary conditions.

In the case of RBF collocation discretizations, boundary conditions can yield stability problems since they destroy the symmetry properties of the operator (cf. [42]), and for RBF-Galerkin discretizations, highly accurate numerical quadrature methods may be required to evalute integrals over non-trivial domains. For that reason, we prefer to choose basis functions that decay sufficiently fast and to not impose boundary conditions on our discretization matrix. Then, the RBF interpolant will automatically have the property that the solution is square integrable. Of course, we still need to place the center points in such a way that we resolve the solution in the domain where the probability distribution is concentrated. From numerical experiments it was observed that a failure to resolve the significant part of the solution can lead to fast oscillations close to the boundary of the resolved domain. In the convergence analysis presented in Sec. 4 we will consider boundary effects in more detail. Note that the Galerkin approach is also more suited for a formulation without explicit boundary conditions since the method includes the inner products of the basis functions in the whole domain while collocation only considers the evaluation points.

2.4 Temporal propagation

After discretizing in space, we have to solve the system of ordinary differential equations (7). For the time-dependent Schrödinger equation there are very efficient explicit propagation methods that are based on the exponential form

$$\lambda(t+\Delta t) = \exp\left(-\frac{\mathrm{i}}{\hbar}M^{-1}G\Delta t\right)\lambda(t). \tag{10}$$

If the Hamiltonian is time-independent, this is an exact formula for the solution. Otherwise, the Magnus expansion [3] gives a series expansion expression based on the exponential form that can be truncated for numerical purposes. The matrix exponential times a vector can be efficiently evaluated based on the Lanczos algorithm [26]. If we propagate $\tilde{\lambda} = R\lambda$, where R is the Cholesky decomposition of the mass matrix, $M = R^*R$, we moreover avoid the computation of the inner product induced by M in the Krylov iterations. This was also discussed in [32]. When the mass matrix becomes very ill-conditioned, we employ a modified Cholesky decomposition[1] with a regularization parameter of the order of the machine precision to ensure positive definiteness.

[1]We have used the Matlab implementation by Brian Borchers available through http://www.mathworks.com/matlabcentral/fileexchange/47.

3 Eigenvalue Stability

The Hamiltonian operator $\hat{H}$ is real and symmetric. Hence, its eigenvalues are all real. Combined with the imaginary unit, the differential operator is self-adjoint and has purely imaginary eigenvalues. This gives rise to several characteristic properties of the equation, e.g., L_2-norm conservation of the solution and reversibility in time.

One difficulty when using radial basis functions for time-dependent problems is that the differentiation matrices often have unstable eigenvalues (cf. [42]). Usually, the problem occurs due to boundary conditions. For the TDSE, we do not impose any boundary conditions. However, stability issues arise due to the potential energy. In order to analyze the stability we need to following lemma:

Lemma 1. *Let $W, U \in \mathbb{R}^{n\times n}$ be two (real) symmetric matrices with U having full rank. Then the generalized eigenvalues μ,*

$$\mu U v = W v,$$

are purely real.

Proof. Multiplying with $v \in \mathbb{C}^n \backslash \{0\}$ from the left gives the following expression for μ,

$$\mu = \frac{v^* W v}{v^* U v}.$$

Since $W^* = W$ and $U^* = U$, the imaginary part of μ becomes

$$\Im\mu = \frac{\mu - \mu^*}{2\mathrm{i}} = \frac{1}{2\mathrm{i}} \frac{v^*(W - W^*)v}{v^* U v} = 0. \tag{11}$$

□

Lemma 1 applies to the Galerkin problem because both the matrices G and M defined in equations (8) are real symmetric. The discretization $M^{-1}G$ has thus real eigenvalues, just as the continuous Hamiltonian operator.

Let us now consider collocation as introduced in Sec. 2.1. In this case, the potential causes an asymmetry in the discrete Hamiltonian H. Hence, Lemma 1 does not apply. Indeed, we can get spurious imaginary parts in the eigenvalues of

$$Hv = \mu A v.$$

We consider equation (11) for this case. By splitting the kinetic and potential part of the Hamiltonian, $H = S + \Lambda A$, and using that S is symmetric we get

$$2\mathrm{i}\Im\mu = (\mu - \mu^*) = \frac{v^*(H + H^*)v}{v^* A v} = \frac{v^*(Q - Q^*)v}{v^* A v},$$

where $Q = \Lambda A$. We observe that $\tilde{Q} := Q - Q^* = [\Lambda, A]$ is anti-symmetric. Hence, $\tilde{Q}$ is an orthogonal matrix with pairs of purely imaginary or zero eigenvalues.

An eigenvalue μ is thus real if and only if $v^* \tilde{Q} v = 0$ holds for the corresponding eigenvector, i.e., if v is a linear combination of eigenvectors of Q to eigenvalue zero and the sum of eigenvectors to each pair of purely imaginary eigenvalues.

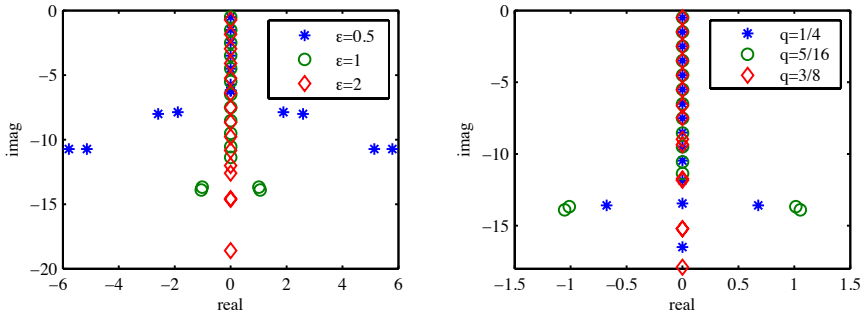

(a) $q = \frac{5}{16}$, various ε. (b) $\varepsilon = 1$, various q.

Figure 1: Eigenvalue spectra for RBF-collocation discretization of the harmonic-oscillator Hamiltonian with 16 basis functions placed uniformly. The eigenvalues for $q = \frac{5}{16}$, $\varepsilon = 2$ adn $\varepsilon = 1$, $q = \frac{3}{8}$ are real.

It is clear that $\tilde{Q}$ is zero if the potential is constant or the matrix A is diagonal. In numerical studies of the eigenvalues, we have observed that it depends on the value of the shape parameter ε and the center point distribution (number of points, size of the region where points are centered/separation radius, and the kind of distribution) whether or not the discretization is eigenvalue stable. For a fixed center point distribution, the eigenvalues become purely imaginary for ε large enough. This is illustrated in Figure 1(a) for the example of a one dimensional harmonic oscillator with 16 nodes placed uniformly with separation radius $q = \frac{5}{16}$. Also, eigenvalue stability can be achieved for increased separation radius (see Figure 1(b)).

3.1 Eigenvectors

The evolution operator of the continuous TDSE is unitary. This ensures norm conservation of the solution. Let us consider the discrete evolution operator for the RBF coefficients in its exponential form $\mathscr{U} = \exp\left(-\frac{\mathrm{i}}{\hbar}U^{-1}W\Delta t\right)$ with $U = M$, $W = G$ for Galerkin and $U = A$, $W = H$ for collocation (cf. (10)). If the eigenvalues of $U^{-1}W$ are real, the norm of $\mathscr{U}$ depends on the eigenvector matrix. To study the eigenvectors, we need the following lemma:

Lemma 2. *Let $W, U \in \mathbb{R}^{n\times n}$ be real symmetric matrices and let U have rank n. Then the eigenvector matrix Q of $U^{-1}W$ is unitary in the U norm, i.e., $Q^*UQ = I_n$.*

Proof. Since U is real and symmetric, we can find its Cholesky decomposition $U = R^*R$. Consider the eigenvalue problem $\mu q = U^{-1}Wq$ and replace U^{-1} by the Cholesky decomposition. Next we multiply by R form the left. This gives

$$\mu Rq = R^{-*}Wq = R^{-*}WR^{-1}Rq.$$

Hence, $Y = RQ$ is the eigenvector matrix of the symmetric matrix $R^{-*}WR^{-1}$ and hence orthogonal. For Q we therefore find

$$I_n = Y^*Y = Q^*R^*RQ = Q^*UQ.$$

□

The lemma applies to the Galerkin discretization and implies that the evolution operator is unitary in the M norm. This means that the M norm of the RBF coefficients is conserved over time. Finally, we have that

$$\lambda^* M \lambda = \psi^* \psi = \|\psi\|_2^2,$$

and the total probability is conserved as in the continuous case. For the collocation matrix on the other hand, firstly the discrete Hamiltonian matrix H is in general not symmetric. Secondly, even if it is, the norm will be based on the interpolation matrix A which does not provide the conservation property. As for the eigenvalues, we again observe that the Galerkin method nicely mimics the properties of the continuous problem.

4 Convergence

Wendland [53] has reported convergence rates of the Galerkin method based on radial basis functions for a linear second-order elliptic equation in a bounded domain. We want to extend this theory to show convergence for the case of the time-dependent Schrödinger equation posed in an unbounded domain. Our reasoning proceeds in three steps: Firstly, we need an estimate for the quality of RBF interpolation. Next, we consider an elliptic problem in an unbounded domain, and finally we introduce the time dependence. The latter two steps are inspired by [50] and would work for any interpolation estimate. The quality of the interpolation thus translates to the quality of the PDE approximation. Convergence for RBF interpolation has been studied by numerous authors. However, for Gaussian basis functions this topic is not yet fully explored for general function spaces. We discuss possible estimates and the underlying assumptions in Sec. 4.1.

4.1 Estimates for interpolation

The estimates for convergence of the solution to the TDSE is based on an estimate for the quality of interpolation for Gaussian RBFs. Estimates for RBF interpolation are usually shown in the native space norm of the corresponding basis function. For a Gaussian φ_ε the native space is defined as

$$\mathcal{N}_G(\mathbb{R}^d) = \left\{ f \in C(\mathbb{R}^d) \cap L_2(\mathbb{R}^d) : \|f\|_{\mathcal{N}_G} := \int_{\mathbb{R}^d} \frac{\left|\hat{f}(\omega)\right|^2}{|\hat{\varphi}_\varepsilon(\omega)|} \mathrm{d}\omega < \infty \right\},$$

where $\hat{}$ denotes the Fourier transform and $\hat{\varphi}_\varepsilon(\omega) = \left(\frac{2\varepsilon^2}{\pi}\right)^{d/4} \exp\left(-\frac{\pi^2\|\omega\|^2}{\varepsilon^2}\right)$. Let $\Omega \subset \mathbb{R}^d$ be an open, bounded domain with C^1-boundary that includes the set X and let h be the fill distance (4). The domain should also satisfy an interior cone condition with an angle ν. According to Thm. 6.4 in [44], it holds for the interpolant I_f of a function $f \in \mathcal{N}(\Omega)$ that

$$\|D^\sigma (f - I_f)\|_{L_2(\Omega)} \leq 2\mathrm{e}^{C\log(h)/\sqrt{h}} \|f\|_{\mathcal{N}(\Omega)}, \tag{12}$$

where D^σ denotes the derivative with multi-index σ and C is a constant depending on σ, ν, d but not on h or f. Note that this estimate does not take into account the conditioning of the interpolation. Depending on the node distribution the condition number can increase severely as h decreases and limit the accuracy that can be achieved in finite precision arithmetic (see [43, 48]).

When posing the problem in $\mathbb{R}^d$, we still choose where to place the nodes and hence which subdomain is properly resolved. Let us denote by Ω_X the convex hull of X and let h_X be the fill distance of Ω_X with respect to X. Then, define $\Omega \supset \Omega_X$ to be an open domain with Lipschitz-continuous and C^1 boundary such that its fill distance equals h_X. For uniform distributions, we will use the domain length L, defined as $2\sqrt[d]{N}q$, i.e., two times the separation radius times the number of grid points per dimension, as characteristic parameter for Ω.

If we want to use this estimate for our convergence proof, we have to assume that both the solution and its temporal derivative are part of the native space during the whole simulation time. Since the native space of Gaussian RBFs is quite small, the shape parameters that can be chosen to obtain convergence for a specific solution is restricted. Therefore, several authors have studied the possibility of finding estimates in Sobolev space norms instead [41, 21, 39]. In [21, 39], it is assumed that the Fourier transform of the basis function satisfies the condition

$$c_1 \left(1 + \|\omega\|_2\right)^{-2\sigma} \leq \hat{\varphi}_\varepsilon(\omega) \leq c_2 \left(1 + \|\omega\|_2\right)^{-2\sigma} \text{ for all } \omega \in \mathbb{R}^d.$$

However, this assumption requires an isomorphism between the native space of the basis functions and a Sobolev space. Hence, the theory does not extend to Gaussian basis functions.

Convergence for analytic functions that are not in the native space was considered by Platte [41], and it is shown that for equidistant node distributions, in one dimension, the convergence behavior of Gaussians follows that of polynomial interpolation.

Let us take a look at the native space. In order for a function to be within the native space of the Gaussian (9), the square root of its Fourier transform needs to decay faster than $\exp\left(-\frac{\pi^2\|\omega\|^2}{\varepsilon^2}\right)$. This means that the native space becomes smaller with decreasing ε (that is, for flatter basis functions). An important class of functions that are part of the native space are the band-limited functions.

Let us consider the special case that f is a complex Gaussian, i.e.,

$$f(x) = \exp\left(-\gamma_1\|x - x_0\|^2 + \mathrm{i}(x - x_0)\gamma_2 + \gamma_3\right).$$

Then, the Fourier transform is given by

$$\hat{f}(\omega) = \left(\frac{\pi}{\gamma_1}\right)^{d/2} \exp\left(-\frac{\pi^2\|\omega - \frac{\gamma_2}{2\pi}\|^2}{\gamma_1} - 2\pi\mathrm{i}x_0\omega + \gamma_3\right).$$

So $f \in \mathcal{N}_G$ holds if $\gamma_1 < 2\varepsilon^2$. For the harmonic oscillator with a coherent state chosen as initial value, the solution will be a complex Gaussian with γ_1 constant over time. Therefore this is a suitable example for studying convergence and the influence of the native space. Figure 2 shows the error as a function of the number of basis functions for various values of ε varying from 0.45 to 0.55. The value of γ_1 is set to 0.5. This means that the solution is part of the native space for $\varepsilon > 0.5$. The same is true for

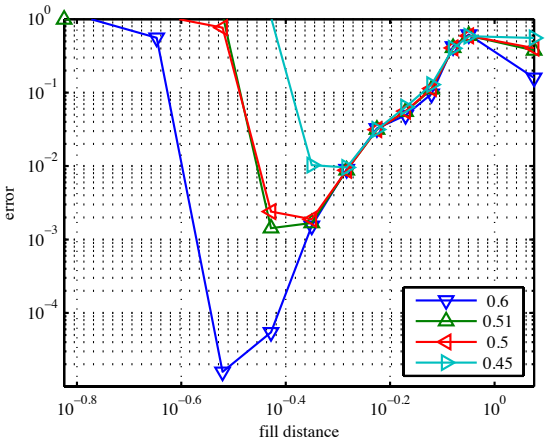

Figure 2: Error as a function of the number of basis functions for various values of the shape parameter. One dimensional harmonic oscillator with coherent initial state, propagation over one period with $p = 0.1$, $x_0 = 0$ initially. The points are spread out equally over a large interval of length 50.

the corresponding time derivatives. We can see that spectral convergence is obtained independent of the value of the shape parameter, especially also for $\varepsilon = 0.5, 0.45$ for which the solution is not within the native space. However, ill-conditioning appears the earlier the smaller the shape parameter is.

4.2 Assumptions

We consider a general form of a time-dependent Schrödinger equation

$$-\sum_{i,j=1}^{d} \frac{\partial}{\partial x_i}\left(b_{ij}(x)\frac{\partial \Psi}{\partial x_j}\right)(x,t) + c(x,t)\Psi(x,t) - \mathrm{i}\Psi_t(x,t) = 0, \quad x \in \mathbb{R}^d, t \in J, \quad (13)$$

where $J = (0, t_{\text{final}}]$, $b_{i,j} \in C^\infty(\mathbb{R}^d)$, $i, j = 1, \ldots, d$ and $B = (b_{ij})$ is symmetric positive definite, and $c \in C^\infty(\mathbb{R}^d \times \overline{J})$. The associated bilinear form is defined as

$$a(\Phi, \Psi; t) = \int_{\mathbb{R}^d} \sum_{i,j=1}^{d} \left(\frac{\partial}{\partial x_j}\Phi(x,t)\right)^* b_{ij}(x) \frac{\partial}{\partial x_i}\Psi(x,t) + \Phi(x,t)^* c(x,t)\Psi(x)\,\mathrm{d}x.$$

We are looking for a weak solution Ψ to

$$a(\Phi, \Psi; t) - \mathrm{i}(\Phi, \Psi_t) = 0 \quad \text{for all } \Phi \in U, t \in J, \quad (14)$$

where $U = \{\varphi \in H^1(\mathbb{R}^d); \|\varphi_t\|_{H^1(\mathbb{R}^d)} < \infty\}$. Note that the assumption that the H^1 norm of the time derivative is bounded is not necessary in general but will be needed for the convergence proof. The initial value $\Psi(x,0) = \Psi_0(x)$ is a given function from U.

We want to find an approximate solution ψ_N in a finite dimensional subspace U_N of U. This finite dimensional subspace is defined by N radial basis functions that are centered at N pairwise distinct points $X \subset \mathbb{R}^d$. Let ψ_N be defined as the solution of

$$a(\varphi, \psi_N) - (\varphi, \psi_{Nt}) = (\varphi, f) \text{ for all } \varphi \in U_N,\ t \in (0, t_{\text{final}}], \quad \psi_N(0) = \psi_0 = I_{\Psi_0}, \tag{15}$$

where the subscript t denotes the temporal derivative. Note that we do not consider temporal discretization here.

In order to show convergence, we have to assume that c is bounded from below, i.e., that there exist a $c_{\min} = \min_{t \in J} \min_{x \in \mathbb{R}^d} c(x,t)$. If $c_{\min}$ is negative, we can transform the problem adding the term $(\delta - c_{\min})\Psi(x,t)$ for a small positive constant δ. Then, the solution of the original problem at time t is given by the solution of the transformed problem times a factor $\exp(\mathrm{i}(\delta - c_{\min})t)$. Therefore, we can assume $c > 0$ in the following without loss of generality. For fixed time t, a then defines a norm on $H^1(\mathbb{R}^d)$ which we denote by $\|\cdot\|_{E_t(\mathbb{R}^d)}$ in the following. Also, it holds that

$$a(\Psi, \Psi) \geq \alpha \|\Psi\|^2_{H^1(\mathbb{R}^d)} \quad \text{for all } \Psi \in U, \tag{16}$$

for a constant $\alpha > 0$ depending on the lower bound of the coefficients of the bilinear form a. Let us denote by $a_\Omega(\cdot,\cdot)$ the bilinear function restricted to the domain Ω. For a bounded set Ω, we also have

$$|a_\Omega(\Phi, \Psi)| \leq \beta \|\Psi\|_{H^1(\Omega)} \|\Phi\|_{H^1(\Omega)} \quad \text{for all } \Phi, \Psi \in U, \tag{17}$$

with constant $\beta > 0$ depending on the upper bound of the coefficients restricted to Ω.

Let Ψ be a function solving equation (14) for a given initial condition. If c is time-independent, it holds that $\frac{\partial}{\partial t} a(\Phi, \Psi) = 0$. This means that the energy of the system is conserved. When c becomes time-dependent, the situation is more intricate. In this case, we have to make additional assumptions: Let us assume that $c(x,t) = c_1(x) + c_2(x,t)$ with $|\frac{\partial}{\partial t} c_2(x,t)| \leq \gamma_1$ for some constant $\gamma_1 > 0$. Then, we have that $a(\Psi(t), \Psi(t)) \leq a(\Psi_0, \Psi_0) + t_f \gamma_1 \|\Psi(t)\|^2_{L^2(\mathbb{R}^d)}$ for $0 \leq t \leq t_f$. Define γ such that $a(\Psi_0, \Psi_0) \leq (\gamma - t_f \gamma_1) \|\Psi_0\|^2_{L_2(\mathbb{R}^d)}$. Since the L_2 norm of a solution of the TDSE is conserved, we then have

$$|a(\Psi, \Psi)| \leq \gamma \|\Psi\|^2_{L_2(\mathbb{R}^d)} \leq \gamma \|\Psi\|^2_{H^1(\mathbb{R}^d)}, \tag{18}$$

where γ depends on the coefficients of the equation and on the initial value. The same reasoning applies to the Galerkin approximation in the subspace U_N. Let us therefore assume that γ is chosen such that the estimate (18) also applies to ψ_N. As a consequence the constant will also depend on I_{Ψ_0}. At first sight, this might be bothersome since I_{Ψ_0} depends on the discretization. However, the quality of the interpolation of the initial value will influence the approximation quality anyway but the interpolation quality of the initial guess will be quite good for a suitably chosen basis.

4.3 Galerkin RBF methods in unbounded domains: elliptic problems

Let us consider the elliptic equation

$$-\sum_{i,j=1}^{d} \frac{\partial}{\partial x_i} \left(b_{ij} \frac{\partial \Psi(x)}{\partial x_j} \right) + c(x)\Psi(x) = f(x), \qquad x \in \mathbb{R}^d, \tag{19}$$

where $f \in H^{-1}(\mathbb{R}^d)$ and $c(x) = c(x,\tau)$ for some fixed value of τ. A weak solution to (19) solves

$$a(\Phi,\Psi) = (\Phi, f), \quad \text{for all } \Phi \in U. \tag{20}$$

Moreover, we define the RBF-Galerkin approximation $\psi_N \in U_N$ as the solution of

$$a(\phi,\psi_N) = (\phi, f), \quad \text{for all } \phi \in U_N. \tag{21}$$

Both Ψ and ψ_N satisfy a relation of type (18) with γ depending on f. Especially, if $f = \mathrm{i}\Psi_t(x,\tau)$ the parameter γ can be found as discussed in Sec. 4.2.

Lemma 3. *Let Ψ be the solution of* (20)*, ψ_N the solution of* (21)*, and Ω the open bounded domain around X defined in Sec. 4.1. Then,*

$$\|\Psi - \psi_N\|_{H^1(\mathbb{R}^d)} \le C \inf_{\phi\in U_N} \left(\|\Psi - \phi\|_{H^1(\Omega)} + \|\Psi - \phi\|_{E_\tau(\mathbb{R}^d\setminus\Omega)} \right). \tag{22}$$

Proof. For any $\phi \in U_N$, it holds that $a(\Psi - \psi_N, \phi) = 0$ (in particular, this holds for $\phi = \psi_N$). Hence, we have for $\phi \in U_N$

$$\begin{aligned}
\|\Psi - \psi_N\|^2_{H^1(\mathbb{R}^d)} &\overset{(16)}{\le} \frac{1}{\alpha} a(\Psi - \psi_N, \Psi - \psi_N) = \frac{1}{\alpha} a(\Psi - \psi_N, \Psi - \phi) \\
&\le \frac{1}{\alpha} \|\Psi - \psi_N\|_{E_\tau(\mathbb{R}^d)} \|\Psi - \phi\|_{E_\tau(\mathbb{R}^d)} \\
&\overset{(17)}{\le} \frac{\beta}{\alpha} \|\Psi - \psi_N\|_{H^1(\mathbb{R}^d)} \|\Psi - \phi\|_{E_\tau(\mathbb{R}^d)}
\end{aligned}$$

Next, we split the energy norm into the part in Ω and the part exterior to the domain and use (18) to find

$$\|\Psi - \psi_N\|_{H^1(\mathbb{R}^d)} \le \frac{\beta}{\alpha} \left(\gamma \|\Psi - \phi\|_{H^1(\Omega)} + \|\Psi - \phi\|_{E_\tau(\mathbb{R}^d\setminus\Omega)} \right).$$

Since ϕ was an arbitrary element of U_N, we have shown the assertion. □

According to estimate (12), we have

$$\|\Psi - I_\Psi\|_{H^1(\Omega)} \le C_{\exp}(h) \|\Psi\|_{\mathcal{N}(\Omega)}, \tag{23}$$

where $C_{\exp}(h)$ is a combination of exponential terms in $\log(h)/\sqrt{h}$. Then, it holds that

$$\begin{aligned}
\|\Psi - \psi_N\|_{H^1(\mathbb{R}^d)} &\overset{(22)}{\le} C \inf_{\phi\in U_N} \left(\|\Psi - \phi\|_{H^1(\Omega)} + \|\Psi - \phi\|_{E_\tau(\mathbb{R}^d\setminus\Omega)} \right) \\
&\le C \|\Psi - I_\Psi\|_{H^1(\Omega)} + C \|\Psi - I_\Psi\|_{E_\tau(\mathbb{R}^d\setminus\Omega)} \\
&\overset{(23)}{\le} C_{\exp}(h) \|\Psi\|_{\mathcal{N}(\Omega)} + C \|\Psi - I_\Psi\|_{E_\tau(\mathbb{R}^d\setminus\Omega)}.
\end{aligned} \tag{24}$$

Here and in the following C denotes a positive constant, not necessarily the same at different occurrences.

To sum up, we see that the Galerkin approximation converges with an exponential rate for the part within the domain Ω. Due to the fact that the solution is posed in

an unbounded domain, we get an additional systematic error whose size is dependent on how well the solution is centered in the domain covered by the basis functions. Important is also how small the interpolant is outside Ω. In [18], it has been shown that the coefficients of a Gaussian radial basis function interpolation on an infinite lattice decay exponentially for the cardinal function. This indicates that the expansion coefficients exhibit some locality. So, if Ψ is small close to the boundary of Ω, we can expect the weights of the basis functions centered close to the boundary in I_ψ to be small, too.

4.4 Galerkin RBF methods in unbounded domains: time-dependent problems

Now, we turn to the case of the time-dependent equation (13) and we consider the semi-discretized system (15). Let us introduce the Ritz projection R_N onto U_N, defined for $w \in U$ by

$$a(\chi, R_N w; t) = a(\chi, w; t), \text{ for all } \chi \in U_N. \tag{25}$$

According to the Riesz representation theorem, there is an $f \in H^{-1}(\mathbb{R}^d)$ such that

$$a(\chi, w; t) = (\chi, f), \text{ for all } \chi \in U.$$

Hence, equation (25) becomes an elliptic problem of the form (21).

Theorem 4. *Let $\Psi \in U$ be the solution of* (14) *and $\psi_N \in U_N$ the solution of* (15)*. Further assume $\Psi|_\Omega, \Psi_t|_\Omega \in \mathcal{N}(\Omega)$. Then, it holds for $t \in [0, t_{\text{final}}]$ that*

$$\begin{aligned} \|\psi_N(t) - \Psi(t)\|_{H^0(\mathbb{R}^d)} \le{}& \|\psi_0 - \Psi_0\|_{H^0(\mathbb{R}^d)} + C_{\exp}(h)\|\Psi_0\|_{\mathcal{N}(\Omega)} \\ &+ C\|\Psi_0 - I_{\Psi_0}\|_{E_0(\mathbb{R}^d\setminus\Omega)} + 2C_{\exp}(h)\int_0^t \|\Psi_t(\tau)\|_{\mathcal{N}(\Omega)}\,\mathrm{d}\tau \\ &+ C\int_0^t \|\Psi_t(\tau) - I_{\Psi_t(\tau)}\|_{E_\tau(\mathbb{R}^d\setminus\Omega)}\,\mathrm{d}\tau + C\|\Psi(t) - I_{\Psi(t)}\|_{E_t(\mathbb{R}^d\setminus\Omega)}. \end{aligned} \tag{26}$$

Proof. First, we split the error into two terms:

$$\psi_N(t) - \Psi(t) = \theta(t) + \rho(t), \quad \text{where } \theta = \psi_N - R_N\Psi, \rho = R_N\Psi - \Psi.$$

Since $R_N\Psi$ is the solution of an elliptic problem of the type studied in the previous section, we know by (24) that

$$\begin{aligned} \|\rho(t)\|_{H^0(\mathbb{R}^d)} \le \|\rho(t)\|_{H^1(\mathbb{R}^d)} &\le C_{\exp}(h)\|\Psi(t)\|_{\mathcal{N}(\Omega)} + C\|\Psi(t) - I_{\Psi(t)}\|_{E_t(\mathbb{R}^d\setminus\Omega)} \\ &\le C_{\exp}(h)\int_0^t \|\Psi_t(\tau)\|_{\mathcal{N}(\Omega)}\,\mathrm{d}\tau + C\|\Psi(t) - I_{\Psi(t)}\|_{E_t(\mathbb{R}^d\setminus\Omega)}. \end{aligned} \tag{27}$$

So let us turn to the θ-part. Let $\chi \in U_N$. Then,

$$\begin{aligned} (\chi, \theta_t) + \mathrm{i}a(\chi, \theta; t) &= (\chi, \psi_{N,t}) + \mathrm{i}a(\chi, \psi_N; t) - (\chi, R_N\Psi_t) - \mathrm{i}a(\chi, R_N\Psi; t) \\ &= -(\chi, R_N\Psi_t) - \mathrm{i}a(\chi, \Psi; t) = -(\chi, R_N\Psi_t - \Psi_t). \end{aligned}$$

Setting $\chi = \theta$, we have

$$(\theta, \theta_t) + \mathrm{i}a(\theta, \theta; t) = -(\theta, \rho_t). \tag{28}$$

Summing (28) and its complex conjugate gives

$$2\|\theta\|_{H^0(\mathbb{R}^d)}\frac{\mathrm{d}}{\mathrm{d}t}\|\theta\|_{H^0(\mathbb{R}^d)} = -(\rho_t,\theta)-(\theta,\rho_t) \le 2\|\rho_t\|_{H^0(\mathbb{R}^d)}\|\theta\|_{H^0(\mathbb{R}^d)},$$

and hence $\frac{\mathrm{d}}{\mathrm{d}t}\|\theta\|_{H^0(\mathbb{R}^d)} \le \|\rho_t\|_{H^0(\mathbb{R}^d)}$ or

$$\|\theta(t)\|_{H^0(\mathbb{R}^d)} \le \|\theta(0)\|_{H^0(\mathbb{R}^d)} + \int_0^t \|\rho_t(\tau)\|_{H^0(\mathbb{R}^d)}\,\mathrm{d}\tau. \tag{29}$$

Assuming $\Psi_t|_\Omega \in \mathcal{N}(\Omega)$ and $\Psi_t \in H_1(\mathbb{R}^d)$, we can find as for $\rho(t)$ that

$$\|\rho_t(t)\|_{H^0(\mathbb{R}^d)} \le C_{\exp}(h)\|\Psi_t(t)\|_{\mathcal{N}(\Omega)} + C\|\Psi_t(t) - I_{\Psi_t(t)}\|_{E_t(\mathbb{R}^d\setminus\Omega)}.$$

Moreover, we estimate $\theta(0)$ by

$$\begin{aligned}\|\theta(0)\|_{H^0(\mathbb{R}^d)} &= \|\psi_0 - R_N\Psi_0\|_{H^0(\mathbb{R}^d)}\\ &\le \|\psi_0-\Psi_0\|_{H^0(\mathbb{R}^d)} + \|\Psi_0 - R_N\Psi_0\|_{H^0(\mathbb{R}^d)}\\ &\le \|\psi_0-\Psi_0\|_{H^0(\mathbb{R}^d)} + C_{\exp}(h)\|\Psi_0\|_{\mathcal{N}(\Omega)} + C\|\Psi_0 - I_{\Psi_0}\|_{E_0(\mathbb{R}^d\setminus\Omega)}.\end{aligned}$$

Hence, (29) becomes

$$\begin{aligned}\|\theta(t)\|_{H^0(\mathbb{R}^d)} \le{}& \|\psi_0-\Psi_0\|_{H^0(\mathbb{R}^d)} + C_{\exp}(h)\|\Psi_0\|_{\mathcal{N}(\Omega)} + C\|\Psi_0 - I_{\Psi_0}\|_{E_0(\mathbb{R}^d\setminus\Omega)}\\ &+ C_{\exp}(h)\int_0^t \|\Psi_t(\tau)\|_{\mathcal{N}(\Omega)}\,\mathrm{d}\tau + C\int_0^t \|\Psi_t(\tau) - I_{\Psi_t(\tau)}\|_{E_\tau(\mathbb{R}^d\setminus\Omega)}\,\mathrm{d}\tau.\end{aligned} \tag{30}$$

Combing (27) and (30) gives the assertion. □

The result of Thm. 4 shows that the quality of the solution depends on three factors:

- the quality of the interpolation of the initial value, $\|\psi_0-\Psi_0\|_{H^0(\mathbb{R}^d)} + C_{\exp}(h)\|\Psi_0\|_{\mathcal{N}(\Omega)}$,
- the approximation error accumulated over the time interval with exponential decay in terms of the fill distance, $2C_{\exp}(h)\int_0^t \|\Psi_t(\tau)\|_{\mathcal{N}(\Omega)}\,\mathrm{d}\tau$,
- a systematic error due to the domain truncation including both the wave packet and the interpolant outside Ω: $C\|\Psi_0 - I_{\Psi_0}\|_{E_0(\mathbb{R}^d\setminus\Omega)} + C\|\Psi(t) - I_{\Psi(t)}\|_{E_t(\mathbb{R}^d\setminus\Omega)} + C\int_0^t C\|\Psi_t(\tau) - I_{\Psi_t(\tau)}\|_{E_\tau(\mathbb{R}^d\setminus\Omega)}\,\mathrm{d}\tau$

If we keep the domain Ω constant and decrease the fill distance h, we therefore expect the error to decay exponentially up to a certain point where it flattens out since the systematic error due to domain truncation takes over. As mentioned earlier, numerical ill-conditioning also has a negative effect on the convergence behavior as the number of basis functions increases.

It is natural to distribute the nodes on a domain Ω such that $\Psi|_{\mathbb{R}^d\setminus\Omega}$ is very small. Hence, the systematic error is dominated by the energy norm of I_Ψ rather than Ψ. The part of the RBFs that is significantly larger than zero extends further into the outside domain $\mathbb{R}^d\setminus\Omega$ the flatter the basis functions are, i.e., the smaller the shape parameter. On the other hand, we can observe in practical computations that the Galerkin approximant will also approximate the solution in $\mathbb{R}^d\setminus\Omega$ to some extent. For instance, for a fixed number of nodes, better results can be obtained if the nodes are clustered on

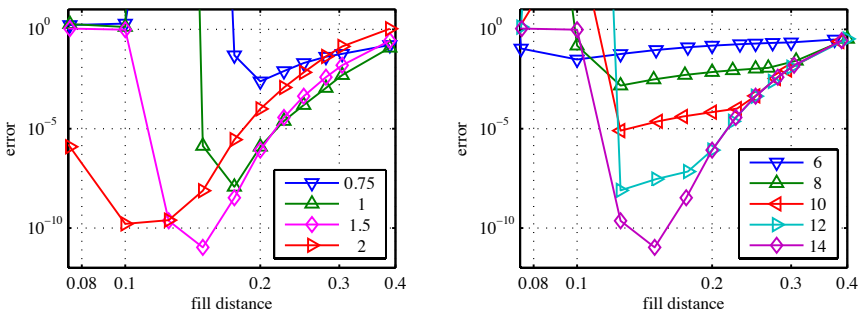

(a) $L = 14$, various ε. (b) $\varepsilon = 1.5$, various L.

Figure 3: Convergence plots for harmonic oscillator propagated over one period.

a smaller domain as the shape parameter decreases. However, this behavior is specific to the Galerkin approximation. Therefore, we believe that the estimation of the systematic error in (26) is pessimistic since it is based on the interpolant.

Remark 5. *For basis functions with native spaces that are isomorphic to a Hilbert space of order k, like for instance Wendland functions, it is possible to show convergence of the order h^k for solutions that are sufficiently smooth up to the point where a systematic error takes over.*

4.5 Numerical evidence

To verify our convergence results numerically, we study the accuracy of an RBF approximation of the 1D harmonic oscillator. We set $x_0 = 0$, $p_{1,0} = 2$, and $m = \omega = 1$. We compute the error after one oscillation at time 2π. First, we compare the convergence for various values of ε for $L = 14$, i.e., for a large domain where the domain truncation error is small compared to other errors in floating point computations. The loglog plot 3(a) reveals exponential convergence up to a point where ill-conditioning takes over. In Figure 3(b), we have plotted the error curves for $\varepsilon = 1.5$ and various values of L. Again, we see the exponential convergence but the smaller L the earlier the systematic error takes over and the error curves flatten out. As the fill distance gets very small, we can again see that the error is increasing due to ill-conditioning. Hence, our numerical results verify the theoretical results developed in this section.

Figure 4 shows how the systematic error goes down as a function of the domain size for the error after propagation as well as for the interpolation of the initial value, when the fill distance is fixed. We report the values for $h \approx 0.15$ where the curves have flattened out. Numerically, we observe exponential convergence also in L for the Galerkin approximation of the solution of the partial differential equation and the interpolant of the initial value.

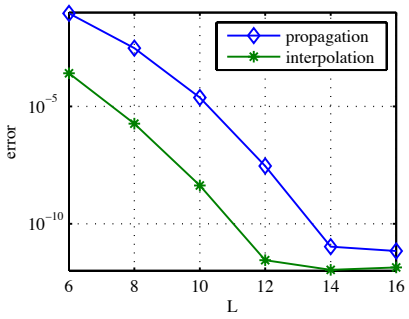

Figure 4: Convergence as a function of the domain size.

5 Transfer between different basis sets

When adapting the basis dynamically to the solution, it becomes necessary to transfer the solution between two basis sets. An accurate basis change is thus a prerequisite for successful adaptation (unless the new node locations can easily be described in terms of a map such as a translation, cf. [15]). In this section, we compare various strategies and their relation to each other. Let $X = \{x_1, \ldots, x_n\}$ and $Y = \{y_1, \ldots, y_m\}$ be two sets of center points. Let us assume we have an RBF-interpolant

$$u(x) = \sum_{i=1}^{n} \lambda_i \varphi_i(\|x - x_i\|).$$

Now, we want to transform this interpolant to one with basis functions centered at the points in Y, i.e., we want to find $\mu = (\mu_1, \ldots, \mu_m)$ such that

$$v(x) = \sum_{i=1}^{n} \mu_i \varphi_i(\|x - y_i\|)$$

and $u(x)$ are close.

We consider three strategies to do so. By A_{UV} we denote the interpolation matrix for center points V and evaluation points U and by M_{UV} the mass matrix for basis functions centered at the points in V and test functions centered in U.

1. Collocation strategy: Evaluate u at the points in Y, $f = (u(y_1), \ldots, u(y_m))^T = A_{YX}\lambda$. Then solve the equation $A_{YY}\mu = f$.
2. Least-squares strategy: Let Z be a set of points with $|Z| > |X|, |Y|$. Evaluate u at the points in Z, $f = (u(z_1), \ldots, u(z_m))^T = A_{ZX}\lambda$. Then solve the equation $A_{ZY}\mu = f$ in least squares sense, that is, solve the normal equations $A_{ZY}^T A_{ZY}\mu = A_{ZY}^T A_{ZX}\lambda$.
3. Galerkin strategy: Solve the equation $M_{YY}\mu = M_{YX}\lambda$.

The collocation strategy yields a new approximant where the difference between u and v is minimal in ℓ_2 sense on the set Y. For the least squares ansatz the difference is minimal in ℓ_2 sense on the set Z.

The relation between the least-squares and the Galerkin strategies can be described as follows. For simplicity, we consider the situation in one dimension. An element

Table 1: Comparison of the interpolation error of a coherent state with $p = 2$ after basis change with Galerkin and collocation strategies, respectively, for various basis sizes (N).

N	Galerkin	collocation
40	$6.9 \cdot 10^{-8}$	$1.1 \cdot 10^{-7}$
30	$3.4 \cdot 10^{-8}$	$5.1 \cdot 10^{-8}$
20	$7.6 \cdot 10^{-5}$	$9.8 \cdot 10^{-5}$
15	$1.5 \cdot 10^{-2}$	$2.4 \cdot 10^{-2}$
10	$3.6 \cdot 10^{-1}$	$8.2 \cdot 10^{-1}$

from the mass matrix reads

$$M_{YY}^{(i,j)} = \int_{\mathbb{R}} \varphi(\|x - y_i\|)^* \varphi(\|x - y_j\|) \, \mathrm{d}x.$$

If we discretize the integral by the trapezoidal rule on an equidistant grid Z with distance Δz between the points, we get

$$M_{YY}^{(i,j)} \doteq \Delta z \sum_{z \in Z} \varphi(\|z - y_i\|)^* \varphi(\|z - y_j\|) = \Delta z (A_{ZY}^* A_{ZY})^{(i,j)}.$$

So we found $M_{YY} \doteq \Delta z A_{ZY}^* A_{ZY}$. Analogously, we can find $M_{YX} \doteq \Delta z A_{ZY}^* A_{ZX}$. In this sense, the normal equation for the least-squares transfer is a discretization of the Galerkin transfer on the grid defined by Z. So the Galerkin transfer is a least-squares transfer in the limit that Z goes to $\mathbb{R}$. In other words, the Galerkin transfer minimizes the error in L_2 sense. Experiments in [32] show that the Galerkin strategy yields very accurate results. In Table 1, we compare the interpolation quality for the transfer of a coherent state with $p = 2$ from a basis with $N = 60$ functions, where the nodes are uniformly distributed over a domain with $L = 12$, onto various smaller basis sets uniformly distributed over an interval of length $L = 10$. The results show that the error is a factor 1.3 to 2.3 smaller when Galerkin projection is used.

6 Parameter Selection

When solving the TDSE with an RBF-Galerkin method, we have a number of parameters that influence the accuracy of the discretization method. The parameters we are concerned with are the total number of basis functions N, the shape parameter ε, and the domain Ω in which the center points are placed (cf. the convergence proof in Sec. 4). Moreover, the distribution of the points within the domain Ω plays an important role. The aim of this section is to numerically analyze how the choice of parameters influences the solution and how sensitive the discretization is to the choice of parameters.

The question of how to choose the shape parameter and the node distribution optimally has been studied extensively, but there are no definitive answers. The placement of nodes can for instance be optimized with a greedy algorithm as proposed by Ling and Schaback [36]. However, this is a costly procedure and it does not take the shape

parameter into account. In our example, two effects regulate the optimal node distribution: On the one hand, it is suitable to concentrate the points in regions where the solution is large, i.e., to adapt the bases to the position of the solution. On the other hand, radial basis function approximations can give improved results in case the nodes are clustered towards the boundary due to the Runge phenomenon and other boundary related effects [20, 43, 19]. For many problems, a Chebyshev distribution of nodes is therefore a good choice [43]. In our case, these two effects are acting conversely since the boundary of the domain is chosen such that the solution is small in this area. For this reason, spreading the nodes on an equidistant grid gives comparably good results for our sample problems. However, we expect this to be less suitable for more advanced problems with less regular structure and in higher dimensions.

The computational cost for computing an RBF approximation is directly coupled to the number of basis functions. However, for the shape parameter the relation to the cost is indirect through the conditioning of the involved matrices. Since the support of the radial basis functions is global, the discretization matrices are dense. In practice the overlap of two basis functions with remote center points is very small and in a numerical setting truncation might be possible. The effect of truncation in the discretization has been studied in the context of the electronic Schrödinger equation with combined Gaussians and polynomials, see [38, 46]. However, we do not consider truncation in this work and aim at choosing the optimal value of the shape parameter in terms of accuracy for a given number of basis functions.

We want to consider the problem of choosing the size of the domain and the (scaled) shape parameter in such a way that we achieve the most accurate result in floating point arithmetics given the number of basis functions. We define the scaled shape parameter as $\alpha = \varepsilon h_{avg}$ where h_{avg} is the average distance between two node points. Note that we use the same scaled shape parameter for all basis functions. This problem can be phrased as an optimization problem. The overall structure of the objective function, the error in the numerical solution as a function of the parameters α and L, is quite simple. However, there are small local variations that make things quite complicated because they give rise to large numbers of local minima. Hence, applying an optimizing routine for smooth functions will not be very successful. Instead, we choose to use a derivative free routine based on coordinate search implemented in Matlab's global optimization toolbox as `patternsearch`.[2]

First of all, we want to consider how the choice of α influences the result for a domain of size $L = 20$ where the error due to domain truncation is insignificant. We consider the example of the harmonic oscillator in one dimension for a coherent state with $p_{1,0} = 2$ and $x_0 = 0$. The lines marked with stars in Figure 5 show the optimal scaled shape parameter as a function of the fill distance and the corresponding error after propagation. We can see that α should be decreased with the fill distance. The increasing values of α for the smallest values of the fill distance are not conclusive because we have then reached the point where the error from the temporal propagation is no longer small in comparison to the spatial errors. Since we will generally not apply an optimization routine before solving a particular problem, we have also added the maximum error attained with a scaled shape parameter in the interval $[\alpha_{\text{opt}} - 0.1, \alpha_{\text{opt}} + 0.1]$ around the optimal value α_{opt} in Figure 5(b). It can

[2] A more sophisticated approach would be to use a derivative-based algorithm in combination with filtering.

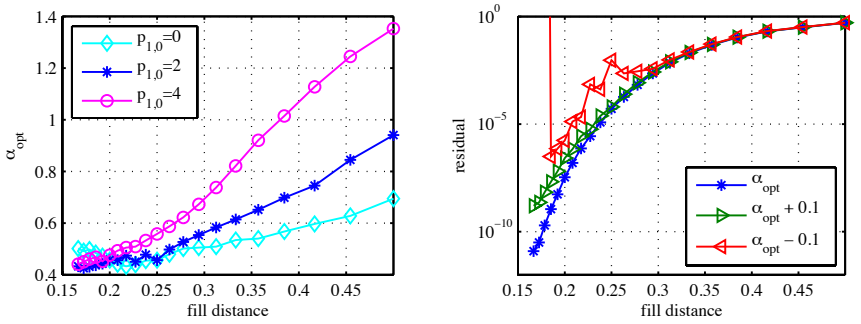

(a) Optimal scaled shape parameter.

(b) Perturbation analysis of parameter choice.

Figure 5: Optimized scaled shape parameter for RBF-Galerkin discretization of the harmonic oscillator in a large domain. Propagation over one period.

be seen that the quality of the method is increasingly sensitive to the shape parameter with decreasing fill distance. It is generally more critical to choose a shape parameter that is too small, especially if the value is already quite small, since this is the most ill-conditioned regime.

Of course, the optimal choice of these values depends on the characteristics of the partial differential equation and its solution: The approximation error for both the solution itself and the operator applied to the solution are of major importance. Generally, it can be said that α should be increased with the variation (e.g. oscillations) in the solution function [35]. This can be observed when comparing the optimal shape parameters for various values of $p_{1,0}$ in Figure 5(a).

Next, we consider both α and L and study the coherent state with $p_{1,0} = 2$ and $x_0 = 0$. The curves marked with circles in Figure 6 show the parameters optimized for an RBF-Galerkin approximation with equidistant nodes and the corresponding error. We can separate three different regions: For five to fifteen nodes, α is decreasing and so is the fill distance. Then, we have another region with fast convergence where the fill distance is kept almost constant and the additional nodes are used to expand the domain. The scaled shape parameter is increasing but at a relatively slow pace. Finally, propagation errors start to dominate at around 45 nodes. This means for very coarse meshes it is preferable to choose rather localized basis functions. As the number of nodes is increased both the domain size should be increased and the fill distance reduced. Eventually, the solution is resolved and it is preferable to increase the computational domain instead of further decreasing the fill distance. It can be seen that the shape parameter is not varying too much in the second region which simplifies the choice.

We have also done the experiment with a Chebyshev distribution of nodes, see the lines marked with squares in Figure 6. Compared to equidistantly distributed nodes the results are comparable in the first region while the convergence for Chebyshev points is slower in the second region. Once the solution is somehow resolved, it is hence preferable to place points on a larger domain rather than clustering them on the boundary. This could be related to Not-a-Knot boundary treatment for problems in bounded domains (cf. [17, 13]).

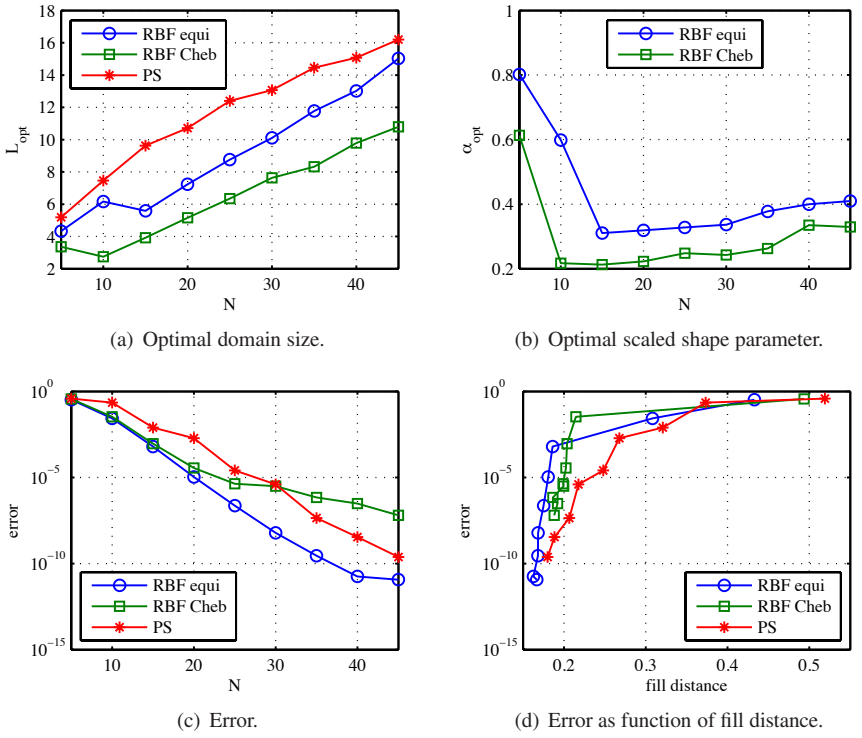

(a) Optimal domain size.

(b) Optimal scaled shape parameter.

(c) Error.

(d) Error as function of fill distance.

Figure 6: Optimized parameters for RBF-Galerkin and pseudospectral discretization of the harmonic oscillator. Propagation over one period.

Again, we want to perform a perturbation analysis, now with respect to both parameters. We choose a perturbation of ± 0.8 for L and ± 0.05 for α. In the first case this corresponds approximately to the change in this parameter when we decrease and increase the number of basis functions by 5 points in the second region. For the scaled shape parameter, on the other hand, this is about half the total variation in the second region. We keep one of the parameters constant at a time and show the worst result obtained in the interval in Figure 7. For the shape parameter, the change is not that dramatic in this case. The choice of L clearly affects the approximation quality.

To sum up, one can say that the choice of parameters is quite important for the quality of the method. We propose to choose the shape parameter rather a little bit too large than too small. Especially, it is usually not commendable to set the scaled shape parameter below 0.3. In the case when the fill distance is small enough to provide reasonable resolution, a scaled shape parameter between 0.3 and 0.5 has shown to be a good choice from our experience. We have also done experiments with a harmonic oscillator in two dimensions. Since the problem and the node distribution were both tensor products, the results are very similar.

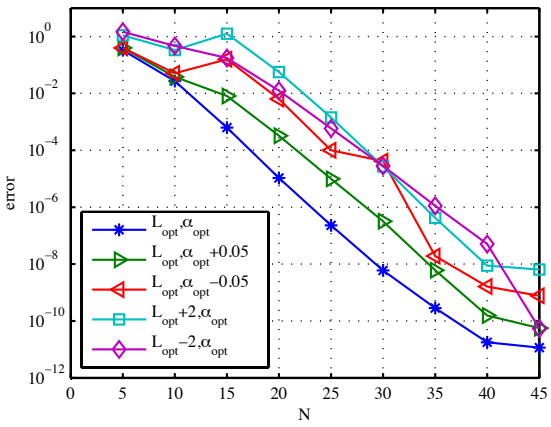

Figure 7: Perturbation analysis for scaled shape parameter and domain size, respectively.

7 Comparison to the Fourier method and RBF-collocation

In order to challenge the RBF approximations, we compare with the Fourier pseudospectral (PS) method [16, 14, 33] which is very common for discretizations of the TDSE. The domain is truncated such that the solution is very small outside the computational domain and then periodic boundary conditions are used. The derivatives can be computed using FFT which gives a complexity of $dn^d \log(n)$ for a d-dimensional grid with n points per dimension. Admittedly, PS methods can be implemented much more efficiently than RBFs where the derivative evaluation has complexity n^{2d} in a naive implementation. On the other hand, RBFs work as well for geometries that are not amenable to tensor product grids and for scattered and adaptive node distributions.

First, we revisit the harmonic oscillator propagated over one period that we have studied in the previous section. Figure 6 also shows how to optimally choose the size of the computational domain and the resulting error for a pseudospectral discretization. It can be seen that an RBF discretization with equidistantly-spaced nodes yields results that are up to two orders of magnitude more accurate compared to the PS result. We observe that the optimal domain size is considerably smaller for radial basis functions. Hence, the separation radius is smaller for RBFs than for PS which explains the gain in accuracy that can be seen from the figures. This is an indication that treating the TDSE without explicit boundary conditions works quite well. However, we have to keep in mind that the RBF discretization is sensitive to the choice of the shape parameter and we get worse results when using non-optimal values of ε.

We have done the same experiment for the two dimensional modified Hénon–Heiles Hamiltonian (2) with $\sigma = 0.2$ and the results are illustrated in Figure 8. The behavior of the parameters and the accuracy are similar as for the harmonic oscillator. In order to compare our Galerkin ansatz to the collocation method, we have also optimized the parameters for the RBF-collocation method. Note that the optimization procedure makes sure that parameters yielding unstable computations are

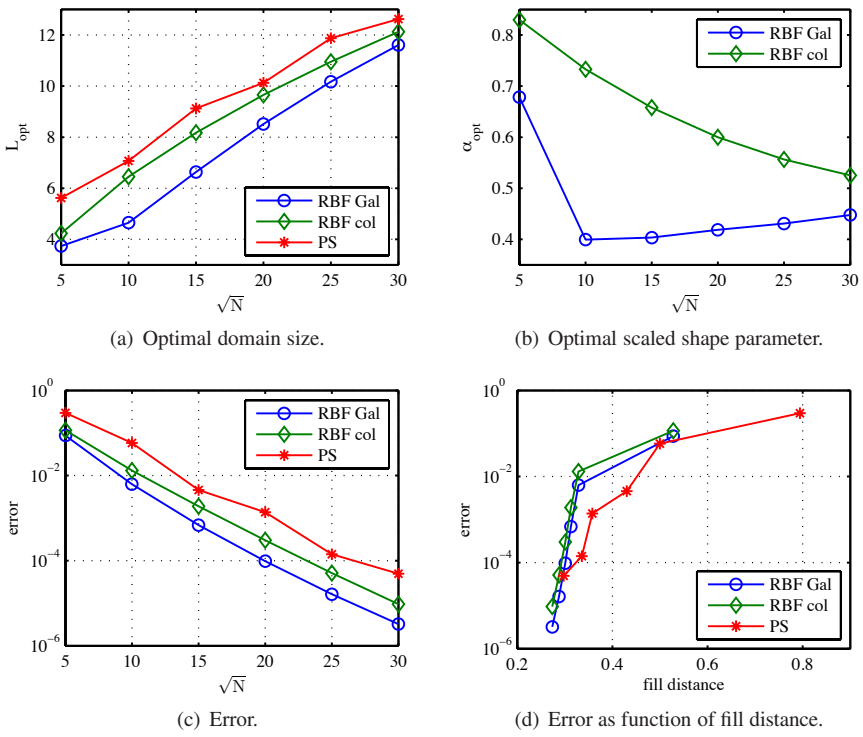

(a) Optimal domain size.

(b) Optimal scaled shape parameter.

(c) Error.

(d) Error as function of fill distance.

Figure 8: Comparison of RBF-Galerkin, RBF-collocation, and pseudospectral discretization of the Hénon–Heiles Hamiltonian. Propagation over time interval of length 1.

avoided. Compared to RBF-Galerkin, larger values are necessary for the domain size as well as the shape parameter. As expected this results in less accurate approximations. Since the approximation matrices in RBF-collocation are not symmetric, the Krylov iterations are slightly more expensive. Hence, the time stepping for the RBF-Galerkin method is a little faster than for RBF-collocation. Again, this supports the supposition that a Galerkin ansatz is superior to collocation when approximating unbounded-domain problems.

8 Conclusions

We have studied RBF-Galerkin discretizations with Gaussian RBFs without explicit boundary conditions. Exponential convergence has been shown theoretically and numerically as long as the nodes are scattered in a large enough domain. Eventually, a systematic error from regions without nodes takes over. A numerical parameter study reveals that the accuracy of the method can be sensitive to the choice of the shape parameter. Especially, the accuracy can deteriorate fast if too small shape parameters are used, which leads to ill-conditioning. Generally, it is not advisable to choose the scaled shape parameter less than about 0.3. In order to obtain the best possible result with a given number of points, the size of the domain where the center points are clus-

tered should be increased linearly with the number of nodes. Typically, the domain can be chosen considerably smaller than for the Fourier method or RBF-collocation. This enables more accurate results for the same number of grid points.

In this article, we have only considered fixed node distributions. However, RBF methods have the potential of being competitive in an adaptive setting where nodes are moved, added, or deleted to accommodate the evolving solution. Especially in high dimensions, the gain in overall problem size from being able to restrict the computational domain to a minimum would be considerable. Truncation of the matrix elements at some threshold is another possibility to consider in order to yield a more memory-efficient implementation of the method.

A Expressions for mass and stiffness matrices

In this section, we collect expressions for the Galerkin matrices for Gaussians of the form (9). We allow for variable ε which can be useful when the nodes are spread out unevenly.

The elements of the mass matrix are:

$$\begin{aligned} M_{jk} &= \int_{\mathbb{R}^d} \varphi_{\varepsilon_j}(\|x-c_j\|)^* \varphi_{\varepsilon_k}(\|x-c_k\|)\,\mathrm{d}x \\ &= \left(\frac{2\varepsilon_j\varepsilon_k}{\varepsilon_j^2+\varepsilon_k^2}\right)^{d/2} \exp\left(-\frac{\varepsilon_j^2\varepsilon_k^2}{\varepsilon_j^2+\varepsilon_k^2}\|c_j-c_k\|^2\right). \end{aligned}$$

The negative Laplacian yields the following stiffness-matrix elements:

$$\int_{\mathbb{R}^d} \nabla\varphi_{\varepsilon_j}(\|x-c_j\|)^* \nabla\varphi_{\varepsilon_k}(\|x-c_k\|)\,\mathrm{d}x = M_{jk}\frac{\varepsilon_j^2\varepsilon_k^2}{\varepsilon_j^2+\varepsilon_k^2}\left(2d-4\frac{\varepsilon_j^2\varepsilon_k^2}{\varepsilon_j^2+\varepsilon_k^2}\|c_j-c_k\|^2\right).$$

A monomial in component ℓ gives:

$$\int_{\mathbb{R}^d} \varphi_{\varepsilon_j}(\|x-c_j\|)^* x_{(\ell)}^p \varphi_{\varepsilon_k}(\|x-c_k\|)\,\mathrm{d}x = M_{j,k}\sum_{q=0}^{\lfloor p/2\rfloor} \beta_{(q)}^{(p)} \frac{\left(\varepsilon_j^2 c_{j,(\ell)}+\varepsilon_k^2 c_{k,(\ell)}\right)^{p-2q}}{\left(\varepsilon_j^2+\varepsilon_k^2\right)^{p-q}},$$

where $\beta^{(0)}=1,\ \beta^{(1)}=1,\ \beta^{(2)}=(1,\frac{1}{2})^T,\ \beta^{(3)}=(1,\frac{3}{2})^T,\ \beta^{(4)}=(1,3,\frac{3}{4})^T,\ \beta^{(5)}=(1,5,\frac{15}{4})^T,\ \beta^{(6)}=(1,\frac{15}{2},\frac{45}{4},\frac{18}{8})^T$.

Considering the case when the potential is interpolated by RBFs, we need to integrate a combination of three Gaussians, leading to:

$$\begin{aligned} &\int_{\mathbb{R}^d} \varphi_{\varepsilon_j}(\|x-c_j\|)^* \varphi_{\varepsilon_\ell}(\|x-c_\ell\|)\varphi_{\varepsilon_k}(\|x-c_k\|)\,\mathrm{d}x = \\ &\left(\frac{\varepsilon_j^2\varepsilon_k^2\varepsilon_\ell^2}{\pi\hat{\varepsilon}^2}\right)^{d/4} \exp\left(-\frac{\varepsilon_j^2\varepsilon_k^2}{\hat{\varepsilon}^2}\|c_j-c_k\|^2-\frac{\varepsilon_j^2\varepsilon_\ell^2}{\hat{\varepsilon}^2}\|c_j-c_\ell\|^2-\frac{\varepsilon_k^2\varepsilon_\ell^2}{\hat{\varepsilon}^2}\|c_k-c_\ell\|^2\right), \end{aligned}$$

where $\hat{\varepsilon}^2=\varepsilon_j^2+\varepsilon_k^2+\varepsilon_\ell^2$.

References

[1] X. Antoine, A. Arnold, C. Besse, M. Ehrhardt, and A. Schädle. A review of transparent and artificial boundary conditions techniques for linear and nonlinear Schrödinger equations. *Commun. Comput. Phys.*, 4:726–796, 2008.

[2] M. Ben-Nun, J. Quenneville, and T. J. Martínez. Ab initio multiple spawning: Photochemistry from first principles quantum molecular dynamics. *J. Phys. Chem. A*, 104:5161–5175, 2000.

[3] S. Blanes, F. Casas, J. Oteo, and J. Ros. The Magnus expansion and some of its applications. *Phys. Rep.*, 470:151–238, 2009.

[4] M. D. Buhmann. *Radial basis functions: theory and implementations*, volume 12 of *Cambridge Monographs on Applied and Computational Mathematics*. Cambridge University Press, Cambridge, 2003.

[5] A. H.-D. Cheng, M. A. Golberg, E. J. Kansa, and G. Zammito. Exponential convergence and *h-c* multiquadric collocation method for partial differential equations. *Numer. Meth. Part. D. E.*, 19:571–594, 2003.

[6] I. Degani. Observations on Gaussian bases for Schrödinger's equation. arXiv:0707.4587v1, 2008.

[7] M. Dehghan and A. Shokri. A numerical method for two-dimensional Schrödinger equation using collocation and radial basis functions. *Comput. Math. Appl.*, 54:136–146, 2007.

[8] W. Dörfler. A time- and space-adaptive algorithm for the linear time-dependent Schrödinger equation. *Numer. Math.*, 73:419–448, 1996.

[9] T. A. Driscoll and A. R. H. Heryudono. Adaptive residual subsampling method for radial basis function interpolation and collocation problems. *Comput. Math. Appl.*, 53:927–939, 2007.

[10] E. Faou and V. Gradinaru. Gauss–Hermite wave packet dynamics: convergence of the spectral and pseudo-spectral approximation. *IMA J. Numer. Anal.*, 29:1023–1045, 2009.

[11] E. Faou, V. Gradinaru, and C. Lubich. Computing semiclassical quantum dynamics with Hagedorn wavepackets. *SIAM J. Sci. Comput.*, 31:3027–3041, 2009.

[12] G. E. Fasshauer. *Meshfree approximation methods with MATLAB*, volume 6 of *Interdisciplinary Mathematical Sciences*. World Scientific Publishing Co. Pte. Ltd., Hackensack, NJ, 2007.

[13] A. I. Fedoseyev, M. J. Friedman, and E. J. Kansa. Improved multiquadric method for elliptic partial differential equations via PDE collocation on the boundary. *Comput. Math. Appl.*, 43:439–455, 2002.

[14] M. D. Feit, J. A. Fleck, Jr., and A. Steiger. Solution of the Schrödinger equation by a spectral method. *J. Comput. Phys.*, 47:412–433, 1982.

[15] N. Flyer and E. Lehto. Rotational transport on a sphere: Local node refinement with radial basis functiions. *J. Comput. Phys.*, 229:1954–1969, 2010.

[16] B. Fornberg. *A Practical Guide to Pseudospectral Methods*. Cambridge University Press, Cambridge, 1996.

[17] B. Fornberg, T. A. Driscoll, G. Wright, and R. Charles. Observations on the behavior of radial basis function approximations near boundaries. *Comput. Math. Appl.*, 43:473–490, 2002.

[18] B. Fornberg, N. Flyer, S. Hovde, and C. Piret. Locality properties of radial basis function expansion coefficients for equispaced interpolation. *IMA J. Numer. Anal.*, 28:121–142, 2008.

[19] B. Fornberg, E. Larsson, and N. Flyer. Stable computations with Gaussian radial basis functions. *SIAM J. Sci. Comput.*, 33:869–892, 2011.

[20] B. Fornberg and J. Zuev. The Runge phenomenon and spatially variable shape parameters in RBF interpolation. *Comput. Math. Appl.*, 54:379–398, 2007.

[21] C. Franke and R. Schaback. Convergence order estimates of meshless collocation methods using radial basis functions. *Adv. Comput. Math.*, 8:381–399, 1998.

[22] D. J. Griffiths. *Introduction to Quantum Mechanics.* Pearson Education, Upper Saddle River, NJ, second edition, 2005.

[23] B.-y. Guo, J. Shen, and C.-l. Xu. Spectral and pseudospectral approximations using Hermite functions: application to the Dirac equation. *Adv. Comput. Math.*, 19:35–55, 2003.

[24] M. Gustafsson, A. Nissen, and K. Kormann. Stable difference methods for block-structured adaptive grids. Technical Report 2011-022, Department of Information Technology, Uppsala University, 2011.

[25] E. J. Heller. Frozen Gaussians: A very simple semiclassical approximation. *J. Chem. Phys.*, 75:2923–2931, 1981.

[26] M. Hochbruck, C. Lubich, and H. Selhofer. Exponential integrators for large systems of differential equations. *SIAM J. Sci. Comput.*, 19:1552–1574, 1998.

[27] L. J. Höök. Kernel density estimation using the RBF-Galerkin method. Technical report, Royal Institute of Technology (KTH), 2012.

[28] X. Hu, T. Ho, and H. Rabitz. Solving the bound-state Schrödinger equation by reproducing kernel interpolation. *Phys. Rev. E*, 61:2074–2085, 2000.

[29] X. Hu, T. Ho, H. Rabitz, and A. Askar. Solution of the quantum fluid dynamical equations with radial basis function interpolation. *Phys. Rev. E*, 61:5967–5976, 2000.

[30] E. J. Kansa. Multiquadrics—a scattered data approximation scheme with applications to computational fluid-dynamics—II. Solutions to parabolic, hyperbolic and elliptic partial differential equations. *Comput. Math. Appl.*, 19:147–161, 1990.

[31] K. Kormann. A time-space adaptive method for the Schrödinger equation. Technical Report 2012-023, Department of Information Technology, Uppsala University, 2012.

[32] K. Kormann and E. Larsson. Radial basis functions for the time-dependent Schrödinger equation. In *Numerical Analysis and Applied Mathematics : ICNAAM 2011*, number 1389 in AIP Conference Proceedings, pages 1323–1326, 2011.

[33] D. Kosloff and R. Kosloff. A Fourier method solution for the time dependent Schrödinger equation as a tool in molecular dynamics. *J. Comput. Phys.*, 52:35–53, 1983.

[34] J. Kucar, H.-D. Meyer, and L. Cederbaum. Time-dependent rotated Hartree approach. *Chem. Phys. Lett.*, 140:525–530, 1987.

[35] E. Larsson and B. Fornberg. Theoretical and computational aspects of multivariate interpolation with increasingly flat radial basis functions. *Comput. Math. Appl.*, 49:103–130, 2005.

[36] L. Ling and R. Schaback. An improved subspace selection algorithm for meshless collocation methods. *Int. J. Numer. Meth. Eng.*, 80:1623–1639, 2009.

[37] S. Manzhos and T. Carrington, Jr. An improved neural network method for solving the Schrödinger equation. *Can. J. Chem.*, 87:864–871, 2009.

[38] P. E. Maslen, C. Ochsenfeld, C. A. White, M. S. Lee, and H. Head-Gordon. Locality and sparsity of ab initio one-particle density matrices and localized orbitals. *J. Phys. Chem. A*, 102:2215–2222, 1998.

[39] F. J. Narcowich and J. D. Ward. Scattered-data interpolation on $\mathbb{R}^n$: Error estimates for radial basis and band-limited functions. *SIAM J. Math. Anal.*, 36:284–300, 2004.

[40] A. Nissen, G. Kreiss, and M. Gerritsen. Stability at nonconforming grid interfaces for a high order discretization of the Schrödinger equation. *J. Sci. Comput.*, 2012.

[41] R. B. Platte. How fast do radial basis function interpolants of analytic functions converge? *IMA J. Numer. Anal.*, 31:1578–1597, 2011.

[42] R. B. Platte and T. A. Driscoll. Eigenvalue stability of radial basis function discretizations for time-dependent problems. *Comput. Math. Appl.*, 51:1251–1268, 2006.

[43] R. B. Platte, L. N. Trefethen, and A. B. J. Kuijlaars. Impossibility of fast stable approximation of analytic functions from equispaced samples. *SIAM Rev.*, 53:308–318, 2011.

[44] C. Rieger and B. Zwicknagl. Sampling inequalities for infinitely smooth functions, with applications to interpolation and machine learning. *Adv. Comput. Math.*, 32:103–129, 2010.

[45] S. Rippa. An algorithm for selecting a good value for the parameter c in radial basis function interpolation. *Adv. Comput. Math.*, 11:193–210, 1999.

[46] E. H. Rubensson and E. Rudberg. Bringing about matrix sparsity in linear-scaling electronic structure calculations. *J. Comput. Chem.*, 32:1411–1423, 2011.

[47] S. A. Sarra. A linear system-free Gaussian RBF method for the Gross-Pitaevskii equation on unbounded domains. *Numer. Meth. Part. D. E.*, 28:389–401, 2012.

[48] R. Schaback. Error estimates and condition numbers for radial basis function interpolation. *Adv. Comput. Math.*, 3:251–264, 1995.

[49] D. Shalashilin and M. Child. Multidimensional quantum propagation with the help of coupled coherent states. *J. Chem. Phys.*, 115:5367–5375, 2001.

[50] V. Thomée. *Galerkin Finite Element Methods for Parabolic Problems*, volume 25 of *Springer Series in Computational Mathematics*. Springer, Berlin, 2nd edition, 2006.

[51] J. A. C. Weideman. Spectral differentiation matrices for the numerical solution of Schrödinger's equation. *J. Phys. A: Math. Gen.*, 39:10229–10237, 2006.

[52] H. Wendland. Piecewise polynomial, positive definite and compactly supported radial functions of minimal degree. *Adv. Comput. Math.*, 4:389–396, 1995.

[53] H. Wendland. Meshless Galerkin methods using radial basis functions. *Math. Comput.*, 68:1521–1531, 1999.

[54] H. Wendland. *Scattered Data Approximation*, volume 17 of *Cambridge Monographs on Applied and Computational Mathematics*. Cambridge University Press, Cambridge, 2005.

[55] Y. Wu and V. S. Batista. Matching-pursuit for simulations of quantum processes. *J. Chem. Phys.*, 118:6720–6724, 2003.